JOC The Journal of Organic Chemistry

Article

pubs.acs.org/joc

A Ligand-Dissociation-Involved Mechanism in Amide Formation of Monofluoroacylboronates with Hydroxylamines

Yuan-Ye Jiang,*[,†,⊥] Chen Wang,[‡,⊥] Yujie Liang,[†] Xiaoping Man,[†] Siwei Bi,*[,†] and Yao Fu*[,§]

[†]School of Chemistry and Chemical Engineering, Qufu Normal University, Qufu 273165, People's Republic of China

[‡]Zhejiang Key Laboratory of Alternative Technologies for Fine Chemicals Process, Shaoxing University, Shaoxing 312000, People's Republic of China

[§]Collaborative Innovation Center of Chemistry for Energy Materials, CAS Key Laboratory of Urban Pollutant Conversion, Department of Chemistry, University of Science and Technology of China, Hefei 230026, People's Republic of China

Supporting Information

ABSTRACT: Acylborons, as a growing class of boron reagents, were successfully applied to amide ligation and showed potential in chemoselective bioconjugation reactions in recent years. In this manuscript, a density functional theory (DFT) study was performed to investigate the mechanism of the amide formation between monofluoroacylboronates and hydroxylamines. An updated pathway was clarified herein, including water-assisted hemiaminal formation, pyridine ligand dissociation, elimination via a six-membered-ring transition state, and water-assisted tautomerization. The proposed mechanism was further examined by applying it to investigate the activation barriers of other monofluoroacylboronates, and the related calculations well reproduced the experimentally reported relative reactivities. On the basis of these results, we found that the ortho substitution of the pyridine ligand destabilizes the acylboron substrates and the hemiaminal intermediates by steric effects and thus lowers the energy demand of the ligand dissociation and elimination steps. By contrast, the para substitution of the pyridine ligand with an electron-donating group enhances the coordination of the ligand by electronic effects, which is a disadvantage to the ligand dissociation and elimination steps. The ligand bearing a rigid linkage blocks the rotation of the pyridine ligand and makes ligand dissociation difficult.

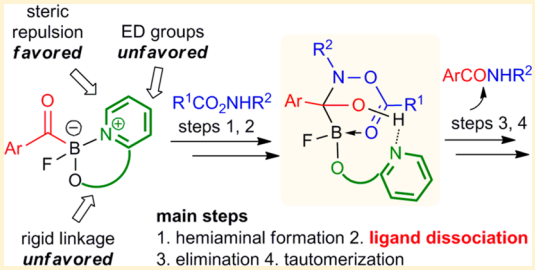

1. INTRODUCTION

The resounding achievement of Suzuki−Miyamura cross-coupling has brought boron reagents, which are widely applied in fine chemical, agrochemical, pharmaceutical, and modern-materials industries,[1] into the holy temple of synthetic reagents nowadays. In contrast to the extensive studies on alkyl, aryl, alkenyl, and alkynyl boron compounds, less attention has been paid to acylborons in early studies as they were envisioned to be too instable.[2] The breakthrough came in 2007, when Yamashita, Nozaki, and co-workers[3] reported of the first fully characterized acylboron that is stabilized by an *N*,*N*-bidentate ligand (Scheme 1a). In the next few years, a number of other acylborons were successfully synthesized or isolated. In 2010, Molander et al.[4] synthesized and isolated potassium acyltrifluoroborate (KAT) (Scheme 1b). Also in 2010, Curran and colleagues[5] reported an *N*-heterocyclic carbene-stabilized acylboron from the reaction of boryl iodide with lithium reagent (Scheme 1c). Thereafter, Yudin et al.[6] disclosed the synthesis of *N*-methyliminodiacetyl (MIDA) acylboronates (Scheme 1d), and Erker et al.[7] isolated formylborane (Scheme 1e). During this period, Bode et al. extended the synthetic methods by which gram-scale preparation of KATs from aldehydes[8] or aryl halides[9] are allowed. Meanwhile, they also disclosed a synthetic route to MIDA acylboronates from KATs in one step.[10] Very recently, Bode et al.[11] made a leap forward and reported new classes of acylboronates that are stable to air, moisture, and silica gel chromatography and can be prepared on gram-scale in one-step from KATs (Scheme 1f). More importantly, this method is compatible with a broad range of ligands (e.g., Schiff bases, 2-(2′-pyridyl)phenol, picolinic acid-derived hydroxamic acid, etc.), and thus, a library of

Scheme 1. Selected Fully Characterized Acylborons

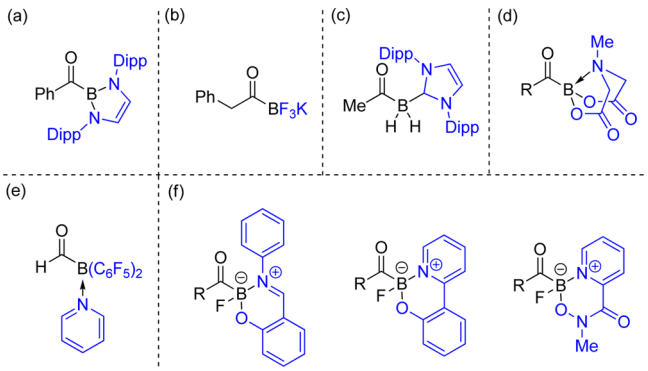

Received: November 1, 2016
Published: December 21, 2016

DOI: 10.1021/acs.joc.6b02642
J. Org. Chem. 2017, 82, 1064−1072

acylboronates with diverse properties and reactivities can be established for further in depth studies.

Encouraged by the preparations and full characterizations, research focusing on exploring the potential utilizations of acylborons has gradually grown. For instance, Erker et al. reported the transformations of formylborane to boryl methanol and alkenylboron compounds.[7] Yudin et al. reported the downstream transformations of MIDA acylborons to borylated heterocycles.[6] As a more attractive application, acylborons were utilized for amide-formation cross-couplings because the conventional amide formation methods involving highly reactive reagents cannot be applied to proteins or protein segments.[12] New acylboron chemistry can provide opportunities for exploring novel biocompatible amide formation reactions to overcome the limitations of the currently available methods such as native chemical ligation.[13] In this context, Molander et al. realized the pioneering amide formation of KATs with azides in 2010 (Scheme 2a).[4]

Scheme 2. Amide Formation of Acylboronates with (a) Azides or (b−d) Hydroxylamines

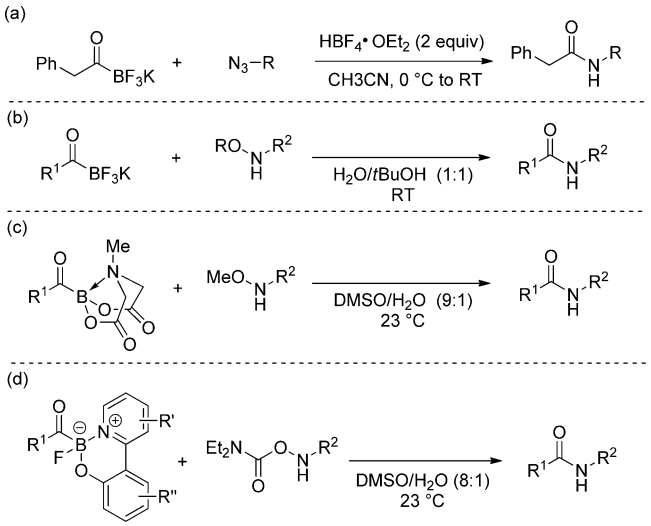

Thereafter, Bode et al. have made contributions to expand amide-forming ligation of acylboronates under aqueous conditions, achieving the cross-couplings of hydroxylamines with KATs[14] (Scheme 2b), MIDA acylboronates (Scheme 2c),[10] and monofluoroacylboronates (Scheme 2d).[11] Furthermore, they successfully synthesized polyethylene glycol (PEG)-based hydrogel via amide ligation between KATs and *O*-carbamoyl hydroxylamines and applied the PEG-based hydrogel to encapsulate bovine chondrocytes, demonstrating the biocompatibility of the KAT ligation.[15]

With the continuous advance of amide formation of acylborons, it was found that the properties of the ligands are critical to the reaction efficiency. For example, according to the product ratio of the reaction in which an equimolar mixture of different monofluoroacylboronates and hydroxylamine **H1** were used, the relative reactivities of monofluoroacylboronates were measured by Bode et al.[11] The relative reactivity of **A1** was set to 100, and different methyl substitutions on the ligands (**A2**, **A3**) can moderately regulate the reactivities (Scheme 3). More remarkably, changing **A1** to **A4** decreases the relative reactivity by 50-fold. As a preliminary mechanism, a pathway involving the addition of hydroxylamine to the carbonyl group to form a

Scheme 3. Relative Reactivity of Different Acylboronates Based on Product Ratio in Their Amide Formation with Hydroxylamime H1[a]

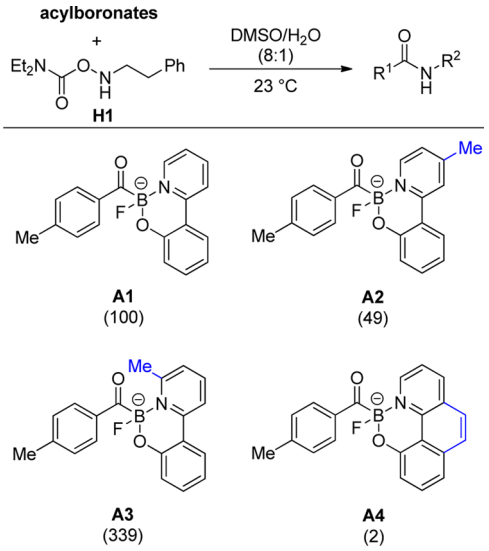

[a]Values are given in parentheses, and the relative reactivity of **A1** is set to 100.

hemiaminal intermediate, concerted elimination to give an imidic acid derivative, and tautomerization to afford amide was proposed by Bode et al. (Scheme 4).[11] The relative stabilities of

Scheme 4. Proposed Mechanism by Bode et al.[11]

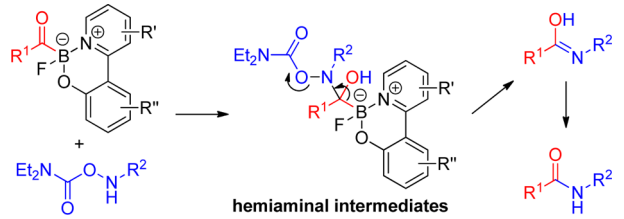

the acylboronate isomers were also investigated with the DFT method, but they were found to not be the sole controlling factor of reactivity, i.e., some less stable isomers also showed lower reactivities. On the basis of these results, Bode et al. proposed that the different performances of **A3** and **A4** arise from different concentrations of their corresponding hemiaminal intermediates.

Fully grasping the reaction mechanism of amide formation of acylboronates, especially elucidating the relationship between reactivities and the properties of ligands, is beneficial to the further development of acylboron chemistry. In this context, a DFT mechanistic study concerning the completed mechanism of amide formation of monofluoroacylboronates with hydroxylamines was conducted in this manuscript. New and corrected insights on the basis of Bode's mechanistic proposal were disclosed. Specifically, the favorable mechanism was found to consist of water-assisted hemiaminal formation, pyridine ligand dissociation, elimination via a six-membered-ring transition state, and water-assisted tautomerization to generate amide. According to our proposed mechanism, the observed relative reactivities of the different monofluoroacylboronates (Scheme 3) are well reproduced. Furthermore, the stabilities of acylboronates and hemiaminal intermediates as well as the

DOI: 10.1021/acs.joc.6b02642
J. Org. Chem. 2017, 82, 1064−1072

Scheme 5. Calculated Energy Profiles of Bode's Mechanism[a]

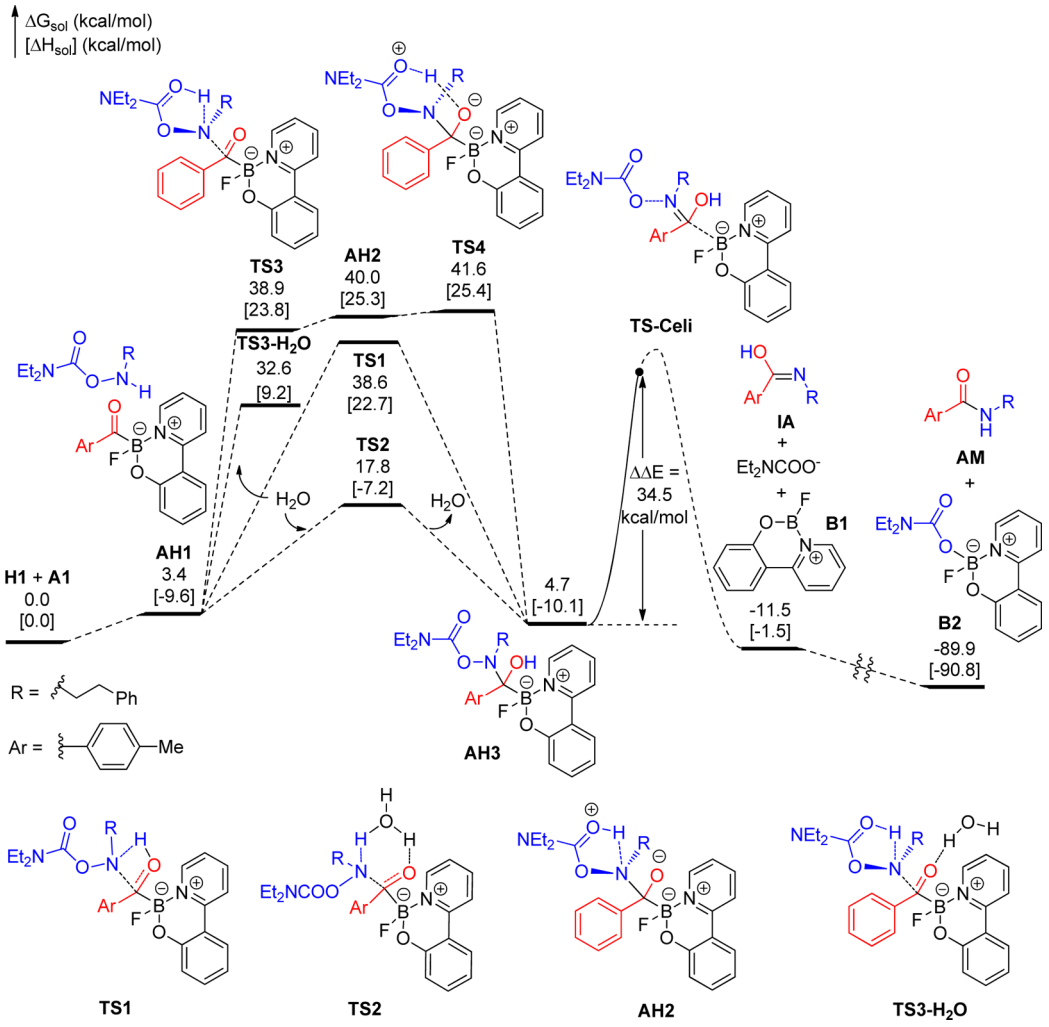

[a]Free energies and enthalpies in brackets are given in kcal/mol.

rate of ligand dissociation are found to both control the reactivities.

2. COMPUTATIONAL METHODS

A DFT study was performed by employing the Gaussian09 program[16] in solution-phase with SMD solvent model[17] (solvent = dimethyl sulfoxide). The M06-2X method,[18] which is recommended by Truhlar et al. for main-group thermochemistry and kinetics, was used in conjunction with an ultrafine integration grid[19] and the basis set def2-SVP developed by Ahlrichs and Weigend.[20] Geometry optimization was conducted without structural restraint unless mentioned otherwise. At the same level of theory, frequency analysis was performed to identify the optimized structures as intermediates (no imaginary frequencies) or transition states (only one imaginary frequency) and also to obtain the thermodynamic corrections at 298.15 K and 1 atm. Intrinsic reaction coordinates (IRC) analysis[21] was conducted to ensure that transition states connect correct intermediates. Then, 1.9 kcal/mol is added to every species to account for the change in standard states from gas phase to solution phase.[22] Natural bond orbital (NBO) analysis was performed with NBO version 3.1 implemented in the Gaussian09 program.[23] The non-covalent interaction plot was obtained by using the program developed by Yang et al.[24] Note that recalculating the solution-phase single point energies with a larger basis set def2-TZVP[20] based on optimized structures was tested. The def2-TZVP-calculated solution-phase single point energies added by def2-SVP-calculated thermodynamic corrections were found to provide the same relative feasibilities for different mechanisms but uniformly overestimate absolute activation barriers. B3LYP[25] associated with def-SVP was tested for some key steps, but it also overestimates the energy barriers (see Tables S1 and S2 for details). Therefore, the solution-phase Gibbs free energies obtained from def2-SVP basis set referring to 298.15 K and 1 mol/L were mainly used in the following discussion unless mentioned otherwise.

3. RESULTS AND DISCUSSION

The amide formation between **A1** and **H1** was first used as a model reaction for mechanistic study. Thereafter, on the basis of the most feasible mechanism, the relative reactivities of **A1**−**A4** in the amide formation with **H1** were evaluated and compared with experimental observations to verify the validity of our calculations and also to explore the factors influencing reactivities.

3.1. Hemiaminal Formation/Concerted Elimination. The mechanistic possibility proposed by Bode et al., which features the formation of a hemiaminal intermediate and the subsequent concerted elimination, was investigated first. As shown in Scheme 5, the combination of **H1** and **A1** generates weakly bound complex **AH1**. This step leads to a slight free energy increase of 3.4 kcal/mol. From **AH1**, hydrogen transfer occurs from the N−H bond of **H1** to the carbonyl oxygen of

DOI: 10.1021/acs.joc.6b02642
J. Org. Chem. 2017, 82, 1064−1072

Scheme 6. (a) Calculated Energy Profile of the Ligand Dissociation/Elimination Mechanism[a] and (b) Optimized Structures of Selected Intermediates and Transition States in the Ligand Dissociation/Elimination Mechanism[b]

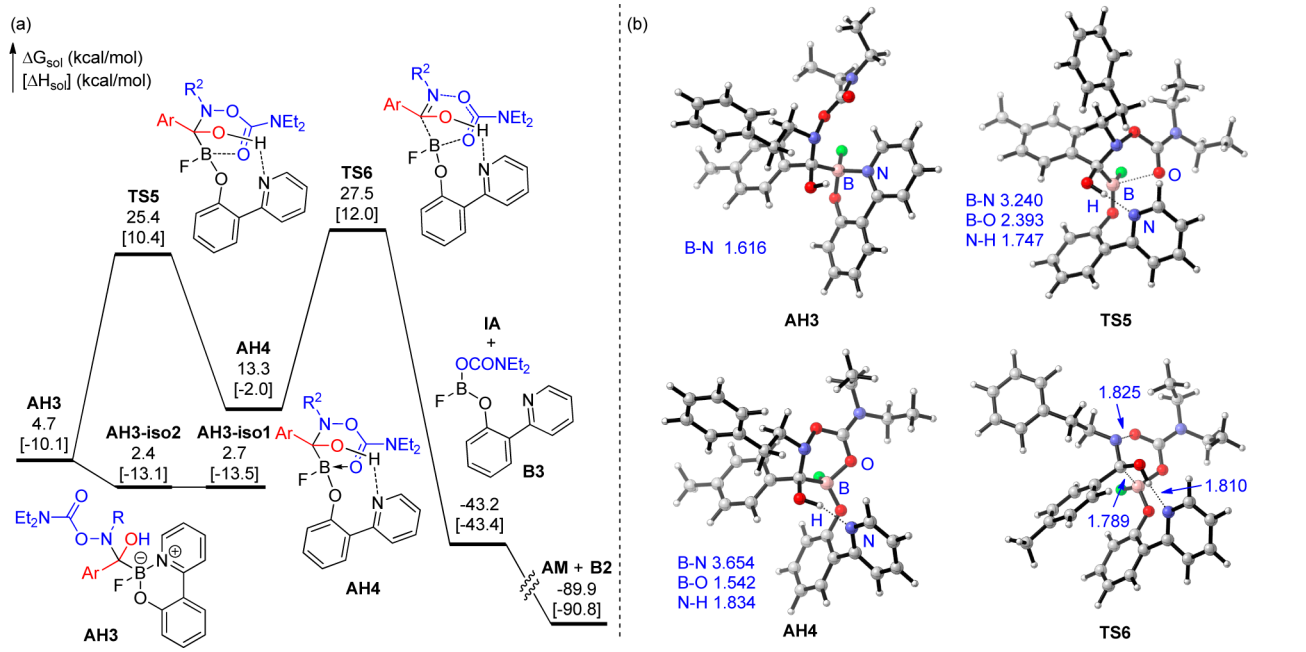

[a]Free energies and enthalpies in brackets are given in kcal/mol. [b]Bond length in angstroms.

A1, and C−N bond formation occurs synchronously. For this process, direct hydrogen transfer via the four-membered-ring transition state **TS1** owns a high overall free energy barrier of 38.6 kcal/mol. Therefore, this direct proton transfer step can be excluded. It is known that proton donors like water and alcohols can promote hydrogen transfer by acting as proton shuttles.[26] Meanwhile, a mixture of dimethyl sulfoxide and water was used in Bode's reactions. Accordingly, the hydrogen transfer is possibly accelerated by the assistance of water. Indeed, the free energy barrier of hydrogen transfer via the water-assisted six-membered-ring transition state **TS2** is lowered to 17.8 kcal/mol. In addition, we considered a stepwise pathway in which the carboxyl group of **H1** initially abstracts the hydrogen atom from the N−H bond of **H1** via five-membered-ring transition state **TS3** to give **AH2**. In **AH2**, an intramolecular hydrogen bond forms between the protonated carboxyl group and the nitrogen atom of the hemiaminal anion with an ═OH···N distance of 1.666 Å. From **AH2**, intramolecular proton transfer proceeds via **TS4** along with the rotation of the protonated carboxyl group to generate the hemiaminal intermediate **AH3**. Because the basicity of hemiaminal anion is much stronger than that of the carboxyl group, the intramolecular proton transfer is nearly barrierless relative to **AH2**. However, the overall free energy barrier of the stepwise pathway **TS3** → **AH2** → **TS4** is too high (>40 kcal/mol) due to the highly instability of the zwitterion **AH2**. Futhermore, we considered adding an extra water to form a hydrogen bond with the carbonyl oxygen to stabilize **TS3** and located **TS3-H_2O**. Although **TS3-H_2O** is indeed more stable than **TS3**, it is still much less favored than **TS2**. Therefore, the stepwise pathway was also excluded for the Bode's experiments that were conducted at room temperature.

Next, concerted elimination on **AH3** via **TS-Celi** to generate imidic acid **IA**, Et_2NCOO^-, and cation **B1** was investigated. Although the free energy change of this process is exergonic by 16.2 kcal/mol, we failed to locate the assumed transition state **TS-Celi**. For the energy demand of this process to be estimated, a relaxed potential surface energy scan of the B−$C_{hemiaminal}$ bond distance was performed (Figure S1). We found that the electronic energy increased by 34.5 kcal/mol when the B−$C_{hemiaminal}$ bond is lengthened to 2.357 Å. Meanwhile, no maximum energetic point was located and no significant N−$O_{carboxyl}$ bond cleavage occurred (N−$O_{carboxyl}$ bond length changes from 1.411 to 1.415 Å) in the elongation of the B−$C_{hemiaminal}$ bond from 1.657 to 2.357 Å. These results suggest that the direct elimination on **AH3** is kinetically unlikely to be possible. The reason can be attributed to the generation of two separately charged species (Et_2NCOO^- and boron cation **B1**) therein, and thus, extra energy is required to overcome the Coulomb interactions between Et_2NCOO^- and **B1**. Indeed, the combination of Et_2NCOO^- and **B1** to generate neutral monofluoroboronate **B2** is highly exergonic by 58.9 kcal/mol. The tautomerization of **IA** to afford amide product **AM** was found to be feasible via a water-assisted proton transfer pathway (Scheme S2). The related free energy barrier is 2.2 kcal/mol, indicating that the tautomerization is facile with the aid of water.

3.2. Hemiaminal Formation/Ligand Dissociation/Elimination. The Bode's mechanistic proposal is problematic in the formation of the amidic acid intermediate because the direct elimination from **AH3** generates unstable charged species Et_2NCOO^- and **B1**. Considering the strong B···O interaction as demonstrated in the last step of Scheme 5, we hypothesize that the dissociation of the 2-(2′-pyridyl)phenolate ligand of **AH3** allows the coordination of the carboxyl group of **H1** to the boron center to form **AH4** (Scheme 6a), and the subsequent elimination via **TS5** will thus be more feasible than that via **TS-Celi** because no formal charged species are generated in the former case. The transformation of **AH3** to **AH4** was found to be a concerted process via **TS5** in which the pyridine ligand dissociates and forms an intramolecular hydrogen bond with the hydroxyl group of the hemiaminal,

DOI: 10.1021/acs.joc.6b02642
J. Org. Chem. 2017, 82, 1064−1072

Scheme 7. Calculated Energy Profile of Ligand Dissociation/Oxoazidines Formation Mechanism[a]

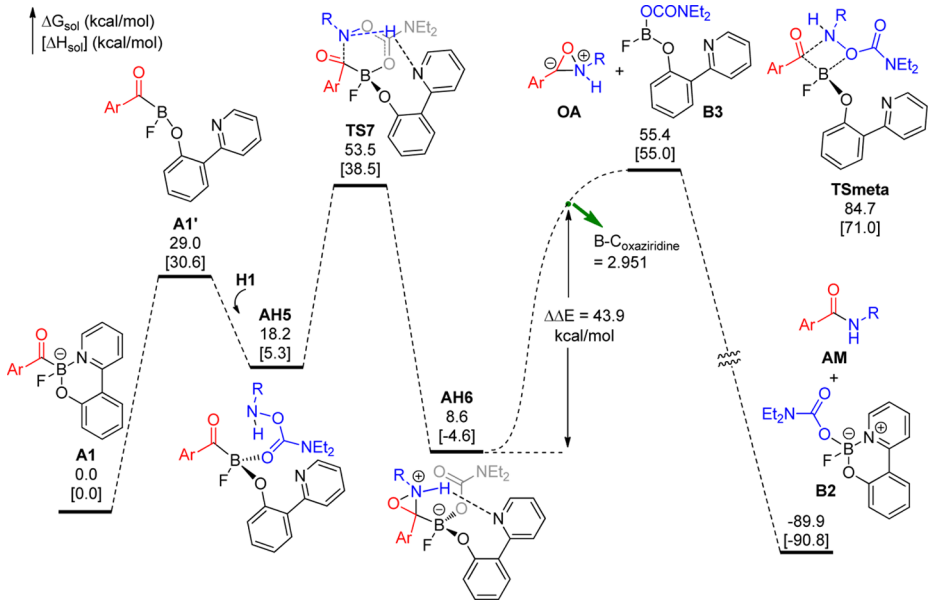

[a]Relative free energies and enthalpies in brackets are given in kcal/mol.

allowing the carboxyl group of the hydroxylamine coordinates to the boron center. In **TS5**, the B−$N_{pyridine}$ distance increases to 3.240 Å, and the B−$O_{carboxyl}$ distance is 2.393 Å (Scheme 6b). Interestingly, the OH···$N_{pyridine}$ distance in **TS5** (1.747 Å) is significantly shorter than that in **AH4** (1.834 Å), suggesting that a stronger intramolecular hydrogen bond is required to overcome the recoordination of the pyridine ligand to the boron center in the transition state. From **AH4**, elimination of amidic acid occurs via the six-membered-ring transition state **TS6**. This step is highly exergonic and generates **IA** and trisubstituted boron **B3**. By comparison, **TS6** is slightly less stable than **TS5** by 2.1 kcal/mol in free energy, and thus, the elimination step is expected to be the rate-determining step in the ligand dissociation/elimination mechanism for the amide formation between **A1** and **H1**. It should be noted that the rotation of the B−C_{acyl} bond of **AH3** can generate two more stable conformational isomers, **AH3-iso1** and **AH3-iso2**, but their associated elimination transition states are both less stable than that of **TS6** (see Scheme S1 for details). Therefore, the overall free energy barrier of the ligand dissociation/elimination mechanism is 27.5 kcal/mol referring to **H1** + **A1**, and the corresponding overall enthalpy barrier is 25.5 kcal/mol referring to **AH3-iso1**. For comparing the ligand dissociation/elimination mechanism with the concerted elimination mechanism (Scheme 4), the electronic energy difference between **TS6** and **AH3** is also checked and found to be 24.0 kcal/mol, which is remarkably lower than the electronic energy demand of concerted elimination (>34.5 kcal/mol). Therefore, we concluded that the ligand dissociation/elimination mechanism is more favorable than the concerted elimination mechanism due to the strong B···$O_{carboxyl}$ bonding in **TS6**.

3.4. Ligand Dissociation/Oxaziridine Formation. Inspired by the presence of ligand dissociation in the elimination stage, we further considered the isomerization of **A1** to **A1′**, from which **H1** coordinates to the boron center to yield **AH5** (Scheme 7). At the outset, we speculated that concerted C_{acyl}−N formation/C_{acyl}−B cleavage/N−$O_{carboxyl}$ cleavage could occur on **AH5** via **TS7** to yield **AM** and **B3** directly. In fact, no C_{acyl}−B cleavage processes were located even when we performed restricted geometry optimization by fixing the C_{acyl}−N bond distance to 1.408 Å (the C_{acyl}−N bond length is 1.354 Å in **AM**). Relaxed surface energy scan also indicates a decrease of C_{acyl}−N bond distance from **AH5**, causing an electron energy increase of over 31.6 kcal/mol (Figure S2). Alternatively, **TS7** results in only N−$O_{carboxyl}$ cleavage and generates the oxoazidine intermediate **AH6**. The free energy barrier of the transformation of **AH5** to **AH6** is as high as 35.3 kcal/mol, which is significantly higher than that of the hemiaminal formation via **TS2**. In **TS2**, concerted hydrogen transfer from the amino group to carbonyl group is present, making the rest of the $NEt_2CO_2(R)N$ moiety more negatively charged and the carbonyl group more positively charged. Therefore, nucleophilic attack of the hydroxylamine toward the acyl carbon is feasible. By contrast, no such hydrogen transfer of the N−H bond is involved in **TS6** to promote this pathway (the N−H bond is 1.137 Å in **TS2** and 1.087 Å in **TS6**). The lower nucleophilicity of $NEt_2CO_2(R)NH$ (compared with $NEt_2CO_2(R)N^-$) results in a shorter N−C_{acyl} bond in **TS7** than that in **TS2** (1.494 vs 1.595 Å). On the other hand, the vibration model of imaginary frequency indicates that **TS7** actually resembles substitution of the carboxyl group of hydroxylamine by the acyl oxygen. Consistent with this viewpoint, the N−$O_{carboxyl}$ bond is partially broken with a Wiberg bond order of 0.508, and the N−O_{acyl} bond is partially formed with a Wiberg bond order of 0.408 in **TS7**. In addition to **TS7**, direct amide formation from **A1′** via four-membered-ring transition state **TSmeta** was examined but found to be kinetically inaccessible.

Next, we considered the B−$C_{oxoazidine}$ bond cleavage on **AH6** for the product formation. However, this process was also kinetically impossible as supported by a relaxed surface energy scan (Figure S3). Specifically, electronic energy increases by 43.9 kcal/mol when the B−$C_{oxoazidine}$ bond is enlarged to 2.951 Å from **AH6**. Moreover, no spontaneous N−O bond cleavage of the oxoazidine to form amide product was observed in this process (the N−O bond varies from 1.414 Å in **AH6** to 1.404

DOI: 10.1021/acs.joc.6b02642
J. Org. Chem. 2017, 82, 1064−1072

Å). The relative total free energies of separate oxoazidine derivative **OA** and **B3** are even higher than that of **AH6** by 46.8 kcal/mol. We speculate that the C-deprotonated **OA** is a strong nucleophile toward boron. Therefore, separating **OA** from **B3** causes a high and continuing electronic energy increase. Because of the kinetically inaccessible $N-C_{acyl}$ bond formation and $B-C_{oxoazidine}$ bond cleavage, we excluded the ligand dissociation/oxoazidine formation mechanism.

3.5. Favorable Mechanism. The results and discussion addressed above support an updated mechanism as the most favorable one among the candidates considered for amide formation between monofluoroacylboronates and hydroxylamines (Scheme 8). In this mechanism, hydroxylamine first

Scheme 8. Updated Mechanism for Amide Formation between Monofluoroacylboronates and Hydroxylamines

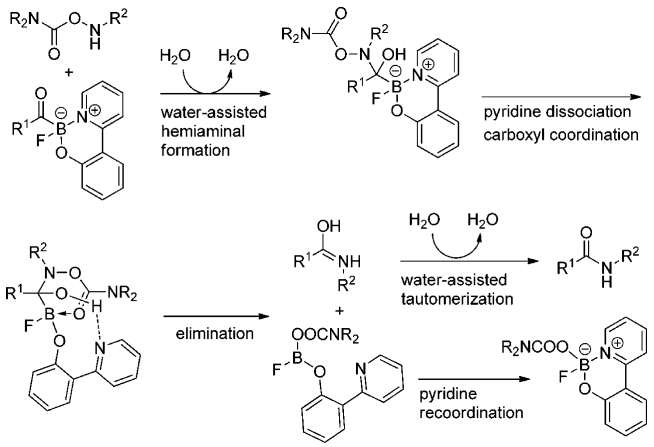

reacts with acylboron to generate a hemiaminal intermediate with the assistance of water. Thereafter, the pyridine ligand dissociates to allow the carboxyl group of hydroxylamine to coordinate with the boron center. Then, elimination occurs via a six-membered-ring transition state to afford an imidic acid from which water-assisted tautomerization occurs to yield the amide product. The feasibility of this renewed mechanism could be mainly attributed to the efficient B···O bonding involved in the elimination transition stgate, which avoids the significant charge separation resulting from the direct elimination. The rate-determining step of the reaction between **H1** and **A1** seems to be the elimination step according to the relative free energies with an overall barrier of 27.5 kcal/mol (referring to **H1** + **A1**). This free energy barrier is overestimated for the reactions conducted at room temperature, but it is understandable because overestimation of the entropy effect generally exists in theoretical studies when the number of molecules changes in the concerned step.[27] If the entropy effect was corrected by using the previously proposed strategy that omits translational and rotational entropies,[28] **AH3-iso2** is more stable than **H1** + **A1** in free energy, and the overall free energy barrier is 25.1 kcal/mol (Scheme S3). Some researchers proposed that the exact contribution of translation and rotation is difficult to determine, and thus, they tend to use enthalpies for mechanistic discussion.[29] The calculated relative enthalpies indicate that **AH3-iso1** is more stable than **H1** + **A1**, and the overall enthalpy barrier is 25.5 kcal/mol. Although the exact overall free energy barrier is unknown due to the uncertainty of the overestimation of entropy effect, the calculated value still lies in an understandable range.

3.6. Origin of the Different Reactivities of Monofluoroacylboronates. For the validity of the calculation results to be verified, the key steps of the amide formation of **A2**−**A4** with **H1** in our proposed mechanism (Scheme 8) were further investigated. The calculated relative free energies and relative enthalpies are summarized in Table 1. Note that the relative reactivities of different acylboronates were measured by Bode et al. according to the amide product ratio of the reaction in which acylboronates and **H1** are all 1.0 equiv. On this occasion, all of the intermediates generated from different acylboronates and **H1** can coexist before rate-determining steps, and **HA-A4-iso** is the most stable one in the mixture of **A1**−**A4** and **H1**. For **A1**−**A3**, the elimination step was found to be the rate-determining step, and the overall free energy

Table 1. Calculated Relative Free Energies and Relative Enthalpies in Brackets for the Amide Formation of Different Acylboronates with H1 (in kcal/mol)[a]

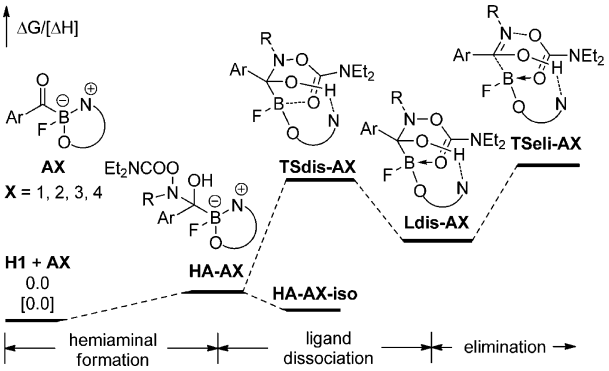

acylborons	HA-AX	HA-AX-iso	TSdis-AX	Ldis-AX	TSeli-AX
A1	4.7/[−10.1]	2.4/[−13.1]	25.4/[10.4]	13.3/[−2.0]	27.5/[12.0]
A2	4.1/[−10.0]	−0.0/[−15.6]	25.4/[11.2]	13.4/[−1.1]	27.6/[12.8]
A3	6.7/[−9.3]	3.5/[−12.8]	21.5/[6.6]	8.9/[−5.7]	23.9/[9.1]
A4	4.1/[−10.7]	−0.9/[−17.3]	32.4/[16.7]	18.1/[1.7]	27.6/[11.6]

[a]**HA-A1** equals **AH3**, **HA-A1-iso** equals **AH3-iso2**, **TSdis-A1** equals **TS5**, **Ldis-A1** equals **AH4**, and **TSeli-A1** equals **TS6**. Conformational isomers of **HA-AX** were considered, and the most stable one in free energy was present as **HA-AX-iso**. For details, see Scheme S4.

DOI: 10.1021/acs.joc.6b02642
J. Org. Chem. 2017, 82, 1064−1072

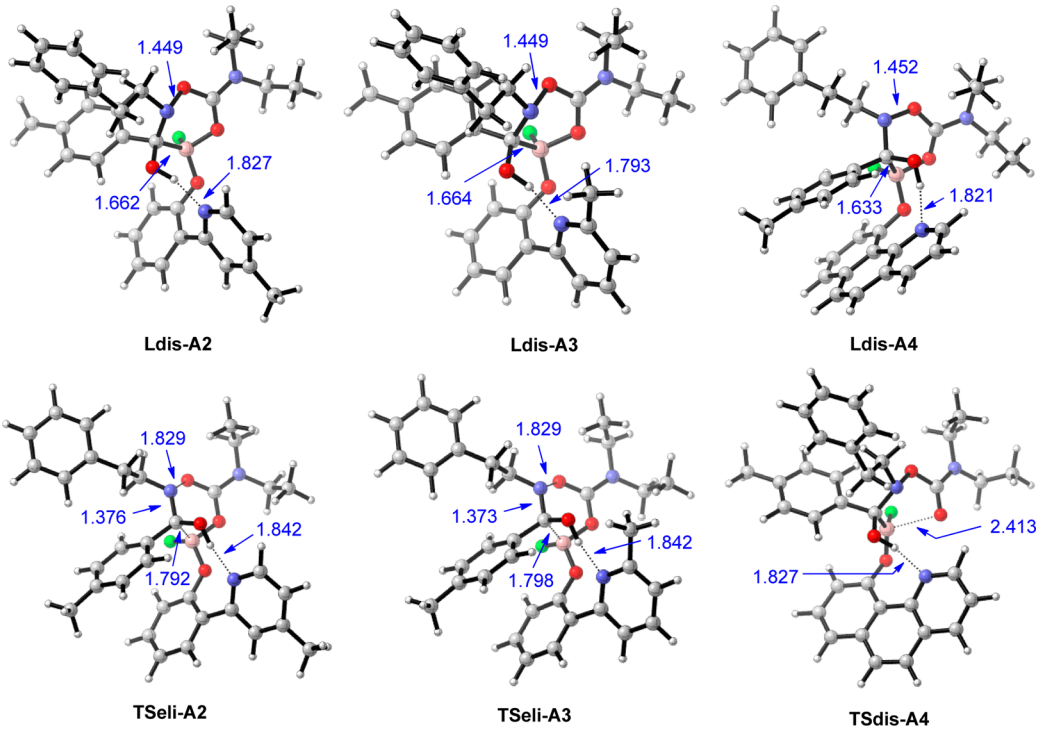

Figure 1. Selected optimized structures of intermediates and transition states in the amide formation of **A2**-**A4** with **H1** (bond length in angstroms).

barriers are 28.4, 28.5, and 24.8 kcal/mol, respectively (refers to **HA-A4-iso**). Interestingly, their free energy barriers of ligand dissociation also predict the same trend for the three acylboronates. To our surprise, the relative free energy of the elimination transition state for **A4** (27.6 kcal/mol) is almost the same as those for **A1** and **A2** (27.5 and 27.6 kcal/mol, respectively). This result suggests that if the steps before the elimination step are feasible, **A4** should exhibit similar reactivity with **A1** and **A2**. Nevertheless, the ligand dissociation step for **A4** requires a free energy barrier of 32.4 kcal/mol, which is remarkably higher than the energy demands of both the ligand dissociation and elimination steps of **A1**−**A3**. Accordingly, **A4** shows bad performance overall. On the basis of the overall free energies barriers of **A1**−**A4** (28.4, 28.5, 24.8, and 33.3 kcal/mol referring to **HA-A4-iso**) and transition state theory, the ratio of the rate constants for the four acylboronates are 100:84:454:0.03 at 23 °C, which is qualitatively consistent with the reported product ratio of the four acylboronates (100:49:339:2 in Scheme 3), giving support for our proposed mechanism.

Further analysis of the energy changes (Table 1) and optimized structures (Figure 1) reveals several factors that control the reactivities of acylborons. First, *para*-electron-donating groups could slightly increase the electron density on the pyridine nitrogen atom of the ligand. Specifically, the NBO charge of the pyridine nitrogen atom is −0.546 in **A1** and −0.554 in **A2**. Accordingly, the coordination of the pyridine ligand toward boron is enhanced. For this reason, the relative free energy and the relative enthalpy of **HA-A2-iso** are lower than those of **HA-A1-iso**, making the energy demand of the ligand dissociation for **A2** relative to **HA-AX-iso** slightly higher than that for **A1**. On the other hand, the enhanced stability of the substrates and intermediates **HA-AX-iso** increases the overall free energy barrier and overall enthalpy barrier for the elimination step, respectively. It should be noted that the *para*-methyl substitution of the pyridine ring also induces a stronger intramolecular hydrogen bond between the pyridine ring and the hydroxyl group in **TSeli-A2** compared with that in **TSeli-A1** (the OH···$N_{pyridine}$ distance is 1.805 Å in **TSeli-A2** and 1.810 Å in **TSeli-A1**, Figure 1). The enhanced intramolecular hydrogen bond does not explain the higher relative energies of **TSeli-A2** than those of **TSeli-A1**, suggesting that the influence of the *para*-methyl substitution on the stabilities of **A2** and **HA-A2-iso** are more significant and slightly decrease the reactivity of **A2** overall.

Second, although the *ortho*-methyl substitution of the pyridine ring (**A3**) also enhances the electron density of the pyridine nitrogen atom, it diminishes the stability of substrates overall due to the steric repulsion of the substituents with the acyl group and the fluoride. In fact, the B−$N_{pyridine}$ bond is 1.619 Å in **A3** and only 1.596 Å in **A2**. **A3** is less stable than **A2** by 3.1 kcal/mol in free energy and by 2.4 kcal/mol in enthalpy, which is in line with the Bode's calculation results.[11a] On this occasion, the overall free energy barrier of the elimination step is decreased. Similarly, because the hemiaminal moiety in **HA-A3** and **HA-A3-iso** are branched while the acyl group in **A3** is planar, the *ortho*-methyl substitution causes stronger steric repulsion in **HA-A3** and **HA-A3-iso** than in **A3**. Therefore, **HA-A3** has higher relative energies than **HA-A2** and **HA-A1**, and **HA-A3-iso** is also less stable than **HA-A1-iso** and **HA-A2-iso**. Because of this factor, the energy barriers of ligand dissociation and the overall enthalpy barrier of the elimination step for **A3** are both decreased. On the other hand, the OH···$N_{pyridine}$ distance is 1.793 Å in **Ldis-A3** and 1.827 Å in **Ldis-A2** (Figure 1), suggesting that the *ortho*-methyl substitution could induce a stronger OH···$N_{pyridine}$ intramolecular hydrogen bond. By contrast, the **TSeli-A3** more approaches a late transition state with a longer OH···$N_{pyridine}$ distance of 1.842 Å, whereas **TSeli-A2** has a shorter OH···$N_{pyridine}$ distance of 1.805 Å. As a result, breaking the hydrogen bond is more significant in the

DOI: 10.1021/acs.joc.6b02642
J. Org. Chem. 2017, 82, 1064−1072

elimination step for **A3** than that for **A2**, making the energetic span between **TSeli-A3** and **Ldis-A3** slightly larger than that between **TSeli-A2** and **TSeli-A2**. Nevertheless, this unfavored electronic effect is overcome by the steric effect-induced instability of the pyridine-coordinated species (**A3**, **HA-A3**, and **HA-A3-iso**).

Third, the rigid ligand benzo[*h*]quinolin-10-olate (in **A4**) encounters difficult ligand dissociation because the rotation of the pyridine moiety is blocked. On this occasion, the ligand dissociation for **A4** requires a larger energy cost. Note that we also checked the direct concerted elimination mechanism (Scheme 4) on **HA-A4** where no ligand dissociation participates. However, this pathway was also found to require an electronic energy demand of over 46.3 kcal/mol (Figure S4) and thus we excluded it. The relative energies of **Ldis-A4** are remarkably higher than those of **Ldis-A1**. Associated with this phenomenon, we found there is repulsion between the bulky benzo[*h*]quinolin-10-olate ligand and the *para*-Me-C_6H_4 group in **Ldis-A4** according to the plot of noncovalent interactions (Figure S5). Therefore, **Ldis-A4** has higher relative free energy and enthalpy, and the energetic span between **TSeli-A4** and **Ldis-A4** is smaller compared with the cases for **A1**−**A3**.

4. CONCLUSIONS

Amide formation by utilizing acylborons opens a new research direction in the area of chemoselective bioconjugation. In this manuscript, a mechanistic study was performed on the amide formation between monofluoroacylboronates and hydroxylamines with the aid of DFT methods. An updated mechanism was determined involving water-assisted hemiaminal formation, dissociation of pyridine ligand, elimination via a six-membered-ring transition state to generate imidic acid, and tautomerization of imidic acid to amide. On the basis of this updated mechanism, the different experimentally observed reactivities of monofluoroacylboronates were reproduced. Both the ligand dissociation and the elimination steps are crucial for the reactivities. The *para* substitution of the pyridine ligand with an electron-donating group enhances the coordination of the pyridine ligand toward boron, slightly increasing the activation barriers of ligand dissociation and elimination. The *ortho* substitution of the pyridine ring with an electron-donating group overcomes the unfavored electronic effect and destabilizes the pyridine-coordinated species to promote the ligand dissociation and elimination steps through a steric effect. Rigid ligands block the rotation of the pyridine ring and hinder the ligand dissociation stage. Overall, this manuscript represents the first theoretical study that clarifies a completed mechanism of amide formation with acylborons. The renewed mechanistic profile not only explains well the observed reactivities but also more importantly sheds light on the origin of ligand effects. We hope the present results inspire further development of acylboron chemistry.

■ ASSOCIATED CONTENT

Supporting Information

The Supporting Information is available free of charge on the ACS Publications website at DOI: 10.1021/acs.joc.6b02642.

Calculated free energies and enthalpies with basis set Def2-TZVP and Def2-SVP, relaxed potential surface scan, calculated energy profile of unfavored pathways, conformational isomers, results based on B3LYP method, and Cartesian coordinates of all optimized structures (PDF)

■ AUTHOR INFORMATION

Corresponding Authors

*E-mail: qfnu_yuanyejiang@163.com.
*E-mail: siweibi@126.com.
*E-mail: fuyao@ustc.edu.cn.

ORCID

Yuan-Ye Jiang: 0000-0002-4763-9173
Yao Fu: 0000-0003-2282-4839

Author Contributions

⊥Y.-Y.J. and C.W. contributed equally to this work.

Notes

The authors declare no competing financial interest.

■ ACKNOWLEDGMENTS

This work was supported by the 973 Program (2012CB215305), the National Natural Science Foundation of China (Nos. 21473100, 21403123, 21325208, 21402181, 21572212), IPDFHCPST (2014FXCX006), CAS (KFJ-EW-STS-051, YZ201563), FRFCU, PCSIRT, Project of Shandong Province Higher Educational Science and Technology Program (No. J14LC17), Opening Foundation of Shandong Provincial Key Laboratory of Detection Technology for Tumor Makers (KLDTTM2015-9), and the Doctoral Start-Up Scientific Research Foundation of Qufu Normal University (Grant No. BSQD2012018). We thank the supercomputer center of USTC for computational support.

■ REFERENCES

(1) (a) Hall, D. G. *Boronic Acids*; Wiley-VCH: Weinheim, 2005. (b) Leonori, D.; Aggarwal, V. K. *Angew. Chem., Int. Ed.* **2015**, *54*, 1082−1096. (c) Lennox, A. J. J.; Lloyd-Jones, G. C. *Angew. Chem., Int. Ed.* **2013**, *52*, 7362−7370. (d) Lennox, A. J. J.; Lloyd-Jones, G. C. *Chem. Soc. Rev.* **2014**, *43*, 412−443. (e) Han, F.-S. *Chem. Soc. Rev.* **2013**, *42*, 5270−5298. (f) Meng, F.; McGrath, K. P.; Hoveyda, A. H. *Nature* **2014**, *513*, 367−374.

(2) (a) Ibrahim, M. R.; Bühl, M.; Knab, R.; Schleyer, P. V. R. *J. Comput. Chem.* **1992**, *13*, 423−428. (b) Schmid, G.; Nöth, H. *Chem. Ber.* **1968**, *101*, 2502−2505. (c) Smith, K.; Swaminathan, K. *J. Chem. Soc., Chem. Commun.* **1975**, 719−720. (d) Smith, K.; Swaminathan, K. *J. Chem. Soc., Dalton Trans.* **1976**, 2297−2300. (e) Stevenson, P. J. In *Comprehensive Organic Functional Group Transformations II*; Katritzky, A. R., Taylor, R. J, Eds.; Elsevier: Oxford, 2005; pp 375−398.

(3) (a) Yamashita, M.; Suzuki, Y.; Segawa, Y.; Nozaki, K. *J. Am. Chem. Soc.* **2007**, *129*, 9570−9571. (b) Segawa, Y.; Suzuki, Y.; Yamashita, M.; Nozaki, K. *J. Am. Chem. Soc.* **2008**, *130*, 16069−16079.

(4) Molander, G. A.; Raushel, J.; Ellis, N. M. *J. Org. Chem.* **2010**, *75*, 4304−4306.

(5) Monot, J.; Solovyev, A.; Bonin-Dubarle, H.; Derat, É.; Curran, D. P.; Robert, M.; Fensterbank, L.; Malacria, M.; Lacôte, E. *Angew. Chem., Int. Ed.* **2010**, *49*, 9166−9169.

(6) He, Z.; Trinchera, P.; Adachi, S.; St Denis, J. D.; Yudin, A. K. *Angew. Chem., Int. Ed.* **2012**, *51*, 11092−11096.

(7) Sajid, M.; Kehr, G.; Daniliuc, C. G.; Erker, G. *Angew. Chem., Int. Ed.* **2014**, *53*, 1118−1121.

(8) Dumas, A. M.; Bode, J. W. *Org. Lett.* **2012**, *14*, 2138−2141.

(9) Erős, G.; Kushida, Y.; Bode, J. W. *Angew. Chem., Int. Ed.* **2014**, *53*, 7604−7607.

(10) Noda, H.; Bode, J. W. *Chem. Sci.* **2014**, *5*, 4328−4332.

(11) (a) Noda, H.; Bode, J. W. *J. Am. Chem. Soc.* **2015**, *137*, 3958−3966. (b) Noda, H.; Bode, J. W. *Org. Biomol. Chem.* **2016**, *14*, 16−20.

DOI: 10.1021/acs.joc.6b02642
J. Org. Chem. 2017, 82, 1064−1072

(12) (a) Kent, S. B. H. *Chem. Soc. Rev.* **2009**, *38*, 338−351. (b) Zheng, J.-S.; Tang, S.; Huang, Y.-C.; Liu, L. *Acc. Chem. Res.* **2013**, *46*, 2475−2484. (c) Saito, F.; Noda, H.; Bode, J. W. *ACS Chem. Biol.* **2015**, *10*, 1026−1033. (d) Bondalapati, S.; Jbara, M.; Brik, A. *Nat. Chem.* **2016**, *6*, 407.
(13) (a) Wang, P.; Dong, S.; Shieh, J. H.; Peguero, E.; Hendrickson, R.; Moore, M. A.; Danishefsky, S. J. *Science* **2013**, *342*, 1357−1360. (b) Okamoto, R.; Mandal, K.; Sawaya, M. R.; Kajihara, Y.; Yeates, T. O.; Kent, S. B. H. *Angew. Chem., Int. Ed.* **2014**, *53*, 5194−5198. (c) Wang, J.-X.; Fang, G.-M.; He, Y.; Qu, D.-L.; Yu, M.; Hong, Z.-Y.; Liu, L. *Angew. Chem., Int. Ed.* **2015**, *54*, 2194−2198. (d) Seenaiah, M.; Jbara, M.; Mali, S. M.; Brik, A. *Angew. Chem., Int. Ed.* **2015**, *54*, 12374−12378.
(14) Dumas, A. M.; Molander, G. A.; Bode, J. W. *Angew. Chem., Int. Ed.* **2012**, *51*, 5683−5686.
(15) Mazunin, D.; Broguiere, N.; Zenobi-Wong, M.; Bode, J. W. *ACS Biomater. Sci. Eng.* **2015**, *1*, 456−462.
(16) Frisch, M. J.; Trucks, G. W.; Schlegel, H. B.; Scuseria, G. E.; Robb, M. A.; Cheeseman, J. R.; Scalmani, G.; Barone, V.; Mennucci, B.; Petersson, G. A.; Nakatsuji, H.; Caricato, M.; Li, X.; Hratchian, H. P.; Izmaylov, A. F.; Bloino, J.; Zheng, G.; Sonnenberg, J. L.; Hada, M.; Ehara, M.; Toyota, K.; Fukuda, R.; Hasegawa, J.; Ishida, M.; Nakajima, T.; Honda, Y.; Kitao, O.; Nakai, H.; Vreven, T.; Montgomery, J. A., Jr.; Peralta, J. E.; Ogliaro, F.; Bearpark, M.; Heyd, J. J.; Brothers, E.; Kudin, K. N.; Staroverov, V. N.; Keith, T.; Kobayashi, R.; Normand, J.; Raghavachari, K.; Rendell, A.; Burant, J. C.; Iyengar, S. S.; Tomasi, J.; Cossi, M.; Rega, N.; Millam, J. M.; Klene, M.; Knox, J. E.; Cross, J. B.; Bakken, V.; Adamo, C.; Jaramillo, J.; Gomperts, R.; Stratmann, R. E.; Yazyev, O.; Austin, A. J.; Cammi, R.; Pomelli, C.; Ochterski, J. W.; Martin, R. L.; Morokuma, K.; Zakrzewski, V. G.; Voth, G. A.; Salvador, P.; Dannenberg, J. J.; Dapprich, S.; Daniels, A. D.; Farkas, O.; Foresman, J. B.; Ortiz, J. V.; Cioslowski, J.; Fox, D. J.; *Gaussian 09*, revision D.01;Gaussian, Inc.: Wallingford, CT, 2013.
(17) Marenich, A. V.; Cramer, C. J.; Truhlar, D. G. *J. Phys. Chem. B* **2009**, *113*, 6378−6396.
(18) Zhao, Y.; Truhlar, D. G. *Theor. Chem. Acc.* **2008**, *120*, 215−241.
(19) For comments on utilizing an ultrafine grid in DFT calculations, see: (a) Gräfenstein, J.; Izotov, D.; Cremer, D. *J. Chem. Phys.* **2007**, *127*, 214103. (b) Johnson, E. R.; Becke, A. D.; Sherrill, C. D.; DiLabio, G. A. *J. Chem. Phys.* **2009**, *131*, 034111. (c) Wheeler, S. E.; Houk, K. N. *J. Chem. Theory Comput.* **2010**, *6*, 395−404. (d) Jiang, Y.-Y.; Man, X.; Bi, S. *Sci. China: Chem.* **2016**, *59*, 1448−1466.
(20) Weigend, F.; Ahlrichs, R. *Phys. Chem. Chem. Phys.* **2005**, *7*, 3297−3305.
(21) (a) Fukui, K. *J. Phys. Chem.* **1970**, *74*, 4161−4163. (b) Fukui, K. *Acc. Chem. Res.* **1981**, *14*, 363−368.
(22) (a) Li, Z.; Zhang, S.-L.; Fu, Y.; Guo, Q.-X.; Liu, L. *J. Am. Chem. Soc.* **2009**, *131*, 8815−8823. (b) Li, H.; Hall, M. B. *J. Am. Chem. Soc.* **2015**, *137*, 12330−12342. (c) Jiang, Y.-Y.; Yan, L.; Yu, H.-Z.; Zhang, Q.; Fu, Y. *ACS Catal.* **2016**, *6*, 4399−4410.
(23) Glendening, E. D.; Reed, A. E.; Carpenter, J. E.; Weinhold, F. *NBO*, version 3.1, 1996.
(24) (a) Johnson, E. R.; Keinan, S.; Mori-Sánchez, P.; Contreras-García, J.; Cohen, A. J.; Yang, W. *J. Am. Chem. Soc.* **2010**, *132*, 6498−6506. (b) Contreras-García, J.; Johnson, E. R.; Keinan, S.; Chaudret, R.; Piquemal, J.-P.; Beratan, D. N.; Yang, W. *J. Chem. Theory Comput.* **2011**, *7*, 625−632.
(25) (a) Becke, A. D. *J. Chem. Phys.* **1993**, *98*, 5648−5652. (b) Lee, C.; Yang, W.; Parr, R. G. *Phys. Rev. B: Condens. Matter Mater. Phys.* **1988**, *37*, 785−789.
(26) See some examples of proton shuttle-assisted hydrogen transfer, see: (a) Goldsmith, B. R.; Hwang, T.; Seritan, S.; Peters, B.; Scott, S. L. *J. Am. Chem. Soc.* **2015**, *137*, 9604−9616. (b) Bach, R. D.; Mattevi, A. *J. Org. Chem.* **2013**, *78*, 8585−8593. (c) Qu, S.; Dang, Y.; Song, C.; Wen, M.; Huang, K.-W.; Wang, Z.-X. *J. Am. Chem. Soc.* **2014**, *136*, 4974−4991. (d) Yuan, B.; He, R.; Shen, W.; Huang, C.; Li, M. *J. Org. Chem.* **2015**, *80*, 6553−6563.
(27) (a) Wertz, D. H. *J. Am. Chem. Soc.* **1980**, *102*, 5316−5322. (b) Leung, B. O.; Reid, D. L.; Armstrong, D. A.; Rauk, A. *J. Phys. Chem. A* **2004**, *108*, 2720−2725. (c) Zhang, S.-L.; Fu, Y.; Shang, R.; Guo, Q.-X.; Liu, L. *J. Am. Chem. Soc.* **2010**, *132*, 638−646. (d) Plata, R. E.; Singleton, D. A. *J. Am. Chem. Soc.* **2015**, *137*, 3811−3826.
(28) For examples estimating the entropy effect by omitting translational and rational contributions, see: (a) Sakaki, S.; Takayama, T.; Sumimoto, M.; Sugimoto, M. *J. Am. Chem. Soc.* **2004**, *126*, 3332−3348. (b) Sumimoto, M.; Iwane, N.; Takahama, T.; Sakaki, S. *J. Am. Chem. Soc.* **2004**, *126*, 10457−10471. (c) Sugiyama, A.; Ohnishi, Y.-y.; Nakaoka, M.; Nakao, Y.; Sato, H.; Sakaki, S.; Nakao, Y.; Hiyama, T. *J. Am. Chem. Soc.* **2008**, *130*, 12975−12985. (d) Jiang, Y.-Y.; Zhang, Q.; Yu, H.-Z.; Fu, Y. *ACS Catal.* **2015**, *5*, 1414−1423.
(29) (a) Jiang, J.; Ramozzi, R.; Morokuma, K. *Chem. - Eur. J.* **2015**, *21*, 11158−11164. (b) Jiang, J.; Yu, J.-Q.; Morokuma, K. *ACS Catal.* **2015**, *5*, 3648−3661. (c) Jiang, J.; Ramozzi, R.; Moteki, S.; Usui, A.; Maruoka, K.; Morokuma, K. *J. Org. Chem.* **2015**, *80*, 9264−9271.

DOI: 10.1021/acs.joc.6b02642
J. Org. Chem. 2017, 82, 1064−1072